RSC Advances

ROYAL SOCIETY OF CHEMISTRY

www.rsc.org/advances

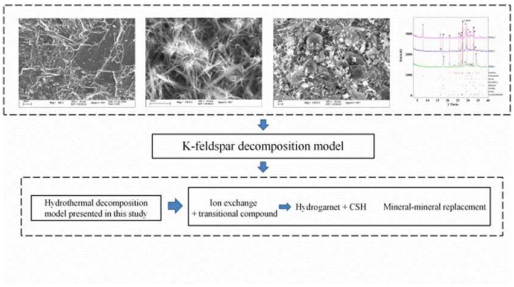

For the first time, a transitional compound [$Ca^{2+}{\equiv}2AlSi_3O_8^-{\equiv}xOH^-$] was observed for K–feldspar hydrothermal alkaline decomposition, and a model was presented.

RSC Advances

ARTICLE

Hydrothermal decomposition of potassium feldspar under alkaline condition

Received 00th January 20xx,
Accepted 00th January 20xx

DOI: 10.1039/x0xx00000x

www.rsc.org/

S. K. Liu[a*], C. Han[a], J. M. Liu[a], and H. Li[b]

Potassium feldspar (K–feldspar) is important for keeping ecological balance on Earth. For example, the weathering of K–feldspar generates dissolved elemental K, a necessary nutrient in soil. Recently, important developments on K-rich feldspar as alternative potash have been reported in a broad spectrum of geographical contexts and soils. Therefore, it is a key point to understand the meachnism of extracting potassium from K-rich rocks such as K–feldspar. The "cook-and-look" experiment cannot completely elucidate the dissolution mechanism of feldspar but can provide a clear idea on physicochemical properties of K–feldspar under some extreme conditions. In this study, the reaction between feldspar and different alkalis under hydrothermal condition was systematically investigated by combining various techniques, such as scanning electron microscopy (SEM), energy-dispersive X-ray spectroscopy, inductively coupled plasma-optical emission spectrometry, X–ray powder diffraction, and the Rietveld method. The deposition of second phases on the surface of K–feldspar was observed by SEM. The reaction process of K–feldspar and $Ca(OH)_2$ was discussed by comparing the reaction between K-feldspar bulk and $Ca(OH)_2$ solution with the reaction between K–feldspar and lime (CaO) powders. A transitional compound $[Ca^{2+} \equiv 2AlSi_3O_8^- \equiv xOH^-]$ for $KAlSi_3O_8$–CaO–H_2O system was observed for the first time. Various phases appeared at different temperatures. Further, a model of K–feldspar decomposition under hydrothermal condition was presented. Studies of K–feldspar hydrothermal reaction provide important and meaningful hints on the utilization of K–feldspar as an alternative to potash, and are helpful for understanding the role of K–feldspar in keeping the ecological balance of the Earth during weathering.

1. Introduction

Water-soluble potassium (K) salts are only abundant in a few countries, such as Canada, Russia, and Belarus. By contrast, water-insoluble K resources, such as K–feldspar, are considerably available worldwide. Therefore, K has to be extracted from K–rich rocks to supply water-soluble K for agriculture in some countries with limited K salts, such as China, Brazil, and India. Recently, important developments on K-rich feldspar as alternative potash have been reported in a broad spectrum of geographical contexts and soils[1-2]. Many authors[3-16] have conducted significant research on extracting K from K-rich feldspar by the hydrothermal reaction of K–feldspar and lime (CaO) in order to look for an alternative of K salts for agriculture. Some researchers[5-7, 9-12] investigated the hydrothermal reaction mechanism of K–feldspar and lime and calculated their thermodynamics and kinetics. Although those papers[5-7, 9-12] have tentatively discussed the reaction

[a] Key Laboratory of Mineral Resources, Institute of Geology and Geophysics, Chinese Academy of Sciences. E-mail: liushanke@mail.iggcas.ac.cn
[b] State Key Laboratory of Lithospheric Evolution, Institute of Geology and Geophysics, Chinese Academy of Sciences.

mechanism of K–feldspar and lime, their conclusions mainly based on X-ray powder diffraction (XRPD) and some deductions in terms of published literatures. Furthermore, those studies did not pay attention to the deposition process of the secondary phase on the surface of K–feldspar, which will be a key point to understand the decomposition of K–feldspar under extreme alkaline condition (e.g., under pressure-tight hydrothermal condition from 160 °C to 220 °C).

Reactions involving feldspars are also important in the environment because of their huge volume in the Earth's crust, and dissolution of feldspars has been widely studied in laboratories to reproduce and understand the processes of "weathering" as observed in the environment[17-19, and references therein]. On the agricultural time scales, the low-temperature dissolution of K–feldspars in non-aggressive aqueous fluids is prohibitively slow, i.e., the mean lifetimes of a 1 mm crystal of K–feldspar in an exogenic cycle are 520000 years[20]. However, the process of chemical reaction is sharply shortened to a few hours or tens of hours for K–feldspar under extreme hydrothermal condition[6, 10, 12-13, 15]. Therefore, the process of K–feldspar decomposition is possibly different for natural weathering and hydrothermal reaction. The "cook-and-look" experiment is an ex-situ way to study a reaction system in an autoclave after the reaction is finished. Therefore, this kind of experiment might not completely illuminate the mechanism of feldspar weathering, and using flow-through systems (in situ) as a classical setup to explore the mechanism of feldspar weathering is not suitable for studying the reaction process of K–feldspar under hydrothermal condition yet. Knowledge of K–feldspar decomposition under both conditions is mutually beneficial for understanding K–feldspar decomposition under different atmospheres.

In this study, the decomposition process of K–feldspar and $Ca(OH)_2$ was investigated by comparing the reaction between K–feldspar bulk and $Ca(OH)_2$ solution with the reaction between K–feldspar and CaO powders under hydrothermal condition, in order to understand the decomposition of K–feldspar under extreme alkaline condition.

2. Experimental protocol

2.1 Materials

K–feldspar was obtained from Shandong Province, China. The sample consisted of microcline and a few impurities, and its chemical composition is shown in Table 1.

Lime (CaO), NaOH, and KOH were all analytical reagents. Considering that lime, NaOH, and KOH absorbed water and CO_2 usually in air, they were roughly weighed first and then dissolved in deionized water. Afterwards, the concentration of each solution was accurately titrated by potassium phthalate. Given that the solubility of lime was very low, $Ca(OH)_2$ solution was prepared at first. NaOH and KOH solutions were then prepared under the prerequisite that the ionic strength and pH of $Ca(OH)_2$, NaOH, and KOH solutions were equal in the same aqueous volume. As a result, the mole numbers of $Ca(OH)_2$, NaOH, and KOH in the same volume had a linear relation, i.e., $N_{Ca(OH)_2} = 2NaOH = 2KOH$.

2.2 Experimental

K–feldspar bulks with a diameter of a few millimeters were prepared and placed into autoclaves. Afterwards, 30 ml fresh NaOH, KOH, and $Ca(OH)_2$ aqueous solutions were respectively added into three autoclaves. These autoclaves were sealed and heated in an electrical furnace. The detailed condition is listed in Table 2.

After the hydrothermal reaction was stopped, the reactors were naturally cooled at room temperature. The K–feldspar bulks were separated from the aqueous solution and washed repeatedly with deionized water. The filtrates were diluted to 100 ml volume with deionized water. Finally, the ion concentration in the filtrated solution was determined by inductively coupled plasma-optical emission spectrometry (ICP–OES) using IRIS advantage inductively coupled argon plasma optical emission spectrometers (Thermo Fisher Scientific Inc., America). Scanning electron microscopy (SEM) using a scanning electron microscope (LEO–1450, Germany) and energy-dispersive X-ray spectroscopy (EDS) using an energy-dispersive X-ray spectrometer (mounted on the scanning electron microscope, Kevex2superdry EDS, USA) were performed for the cleaned feldspar bulks to observe the morphology and to measure the composition after hydrothermal reactions.

To differentiate phases formed during the hydrothermal reaction, a mixture of 5.5 g K–feldspar powder, 4.5 g CaO powder, and 30 ml deionized water was cooked in the autoclaves for 24 h at 160, 190, and 220 °C, respectively. Reactive productions were removed from the autoclaves and heated at 105 °C to evaporate water. The productions for 160, 190, and 220 °C were labeled as PCK–1, PCK–2, and PCK–3, respectively. XRPD patterns of PCK–1, PCK–2, and PCK–3 were collected using a Dmax2400 X-ray diffractometer (Rigaku, Japan) under 40 KV and 80 mA from 3° to 70° at 0.02° per step. Quantitative phase analysis from XRPD was conducted using GSAS[21] and EXPGUI[22] by the Rietveld method[23] for all phases of PCK–1, PCK–2, and PCK–3. SEM was also carried out to observe morphologies. To further analyze physicochemical

Table 1 Chemical composition of K–feldspar (wt%)

SiO_2	TiO_2	Al_2O_3	Fe_2O_3+FeO	MnO	CaO
63.89	0.28	18.07	0.90	0.00	0.06
MgO	K_2O	Na_2O	P_2O_5	Loss	Total
0.00	16.13	0.28	0.03	0.24	99.87

Table 2 Details of hydrothermal reaction between K–feldspar bulk (KFB) and different alkaline solutions with equal basic strength

Sample	KFB Mass/g	Added alkalis		Temperature /°C	Time /h
		alkali	mole/mmol		
NK	2.2257	NaOH	1.42	190	20
KK	2.2114	KOH	1.42	190	20
CK–1	2.2282	$Ca(OH)_2$	0. 71	160	20
CK–2	2.2282	$Ca(OH)_2$	0.71	190	20
CK–3	2.2245	$Ca(OH)_2$	0.71	220	20

Table 3 Ion concentration in the filtrate after hydrothermal decomposition

Sample	Ion amount in filtrate after hydrothermal reaction /mmol				
	K	Si	Al	Ca	Na
NK	0.0463	0.2288	0.0820	0.0061	1.2406
KK	1.2516	0.1253	0.0415	0.0068	0.0911
CK–1	0.0662	0.0036	0.0046	0.3912	0.0130
CK–2	0.1218	0.0276	0.0060	0.2882	0.0224
CK–3	0.1617	0.0218	0.0193	0.0045	0.0160

characteristics of PCK–1, PCK–2, and PCK–3, 2 g sample was weighed for each production. 1 g of 2g sample was mixed into 100 ml deionized water, and another 1 g was mixed into 100 ml 0.5 mol/l HCl. Both solid-liquid mixtures of each production were placed into a constant-temperature oscillator for an hour and then were filtered through a filter paper. The filtrates were analyzed by ICP–OES to measure their ion concentrations.

3. Results and discussion

Ion concentrations in the filtrates measured by ICP–OES were converted into mole numbers, as shown in Table 3. SEM images of K–feldspar attacked by different alkalis are shown in Fig. 1, and chemical compositions of some particles with different morphology measured by EDS are listed in Table 1S‡. XRPD patterns of PCK–1, PCK–2, and PCK–3 are plotted in Fig. 2, and their SEM is shown in Fig. 3. The quantitative phase analysis results of PCK–1, PCK–2, and PCK–3 are listed in Table 2S‡, and oxide contents in the filtrates of PCK–1, PCK–2, and PCK–3 measured by ICP–OES are shown in Table 4.

3.1 Decomposition under different alkalis with the same ionic strength at 190 °C

From Figs. 1A, B, C, and G, the surface of K–feldspar bulk was almost the same as that of the original K–feldspar (OK) after it was attacked by NaOH (NK) and KOH (KK). However, the K–feldspar attacked by $Ca(OH)_2$ (CK–2) presented a different morphology. $Ca(OH)_2$ more easily decomposed K–feldspar among the three alkalis with the same ionic strength. This result was directly related to new phases formed by the reaction between K–feldspar and $Ca(OH)_2$. Nevertheless, no new phase was found on the surface of K–feldspar attacked by NaOH and KOH in this study, and EDS also supported this trend. Chemical compositions for OK, NK, and KK were very close to each other (Table 1S), but the chemical composition of CK–2 significantly differed from those of OK, NK, and KK.

K–feldspar can react with NaOH or KOH solution to form new phases under hydrothermal condition[7, 24]. Therefore, the case in which no new phase appeared for NK and KK in this study should be related to low concentration of NaOH and KOH or/and short-cooked time; new phases would appear if given with a prolonged time, e.g., feldspar formed other phases by a dissolution-reprecipitation process under a fluid system (please refer to extensive reviews in 25-27). However, the reaction between K–feldspar and NaOH or KOH did

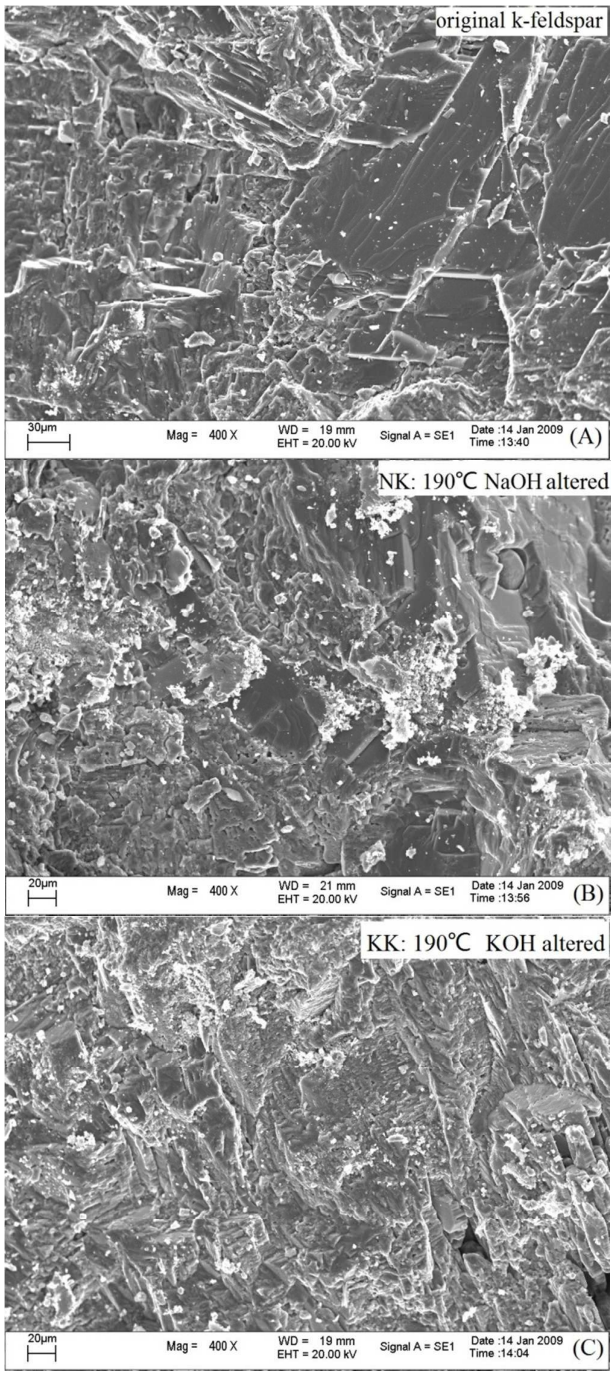

Fig. 1 (A)-(C) SEM of K–feldspar surface: (A) Original K–feldspar (OK); (B) NaOH-altered K–feldspar at 190 °C (NK); (C) KOH-altered K–feldspar at 190 °C (KK).

proceed because some elements, such as K, Al, and Si, were dissolved into the solution (Table 3). The amounts of Al and Si in the filtrate of NK were more than those in the filtrate of KK because of the K^+ common ion effect. Nevertheless, the amounts of Al and Si in the filtrate of CK–2 were less than those in the filtrates of NK and KK because of the precipitation of new phases. The reaction of K–feldspar under different alkalis clearly showed that the decomposition of feldspar was a

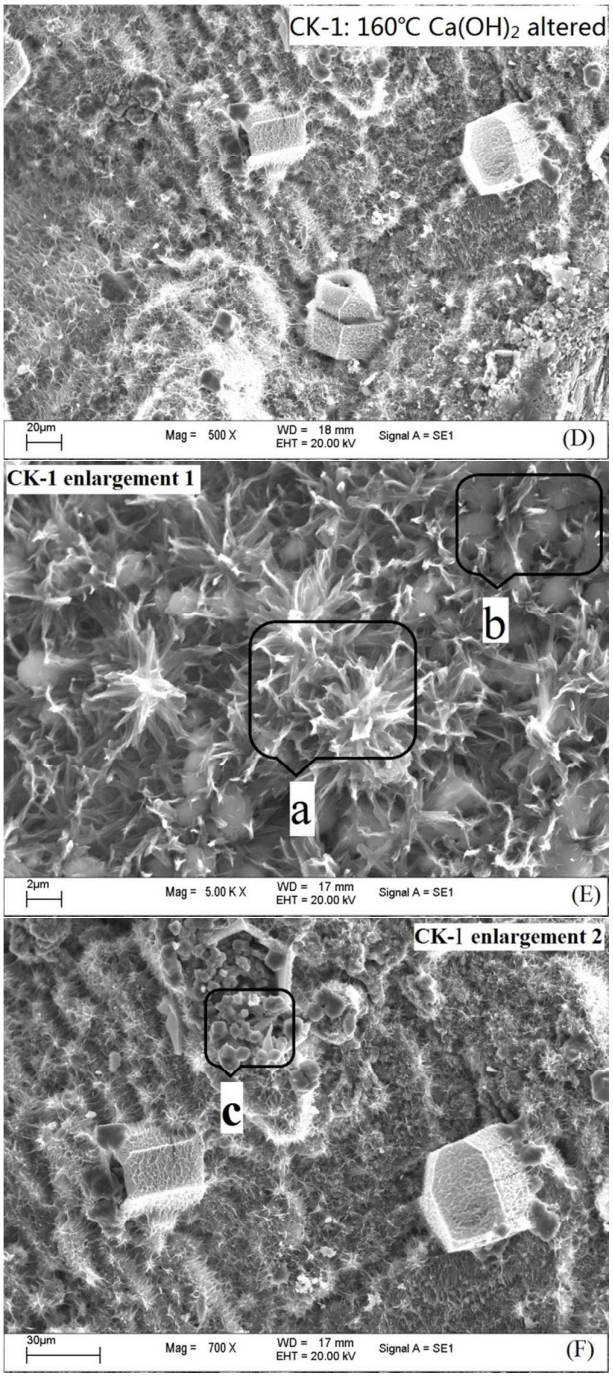

Fig. 1 (D)-(F) SEM of K–feldspar surface: (D) $Ca(OH)_2$-altered K–feldspar at 160 °C (CK–1); (E) Enlargement part one of CK–1 (CK–1a, fiber; CK–1b, spherule); (F) Enlargement part two of CK–1 (CK–1c, polyhedron).

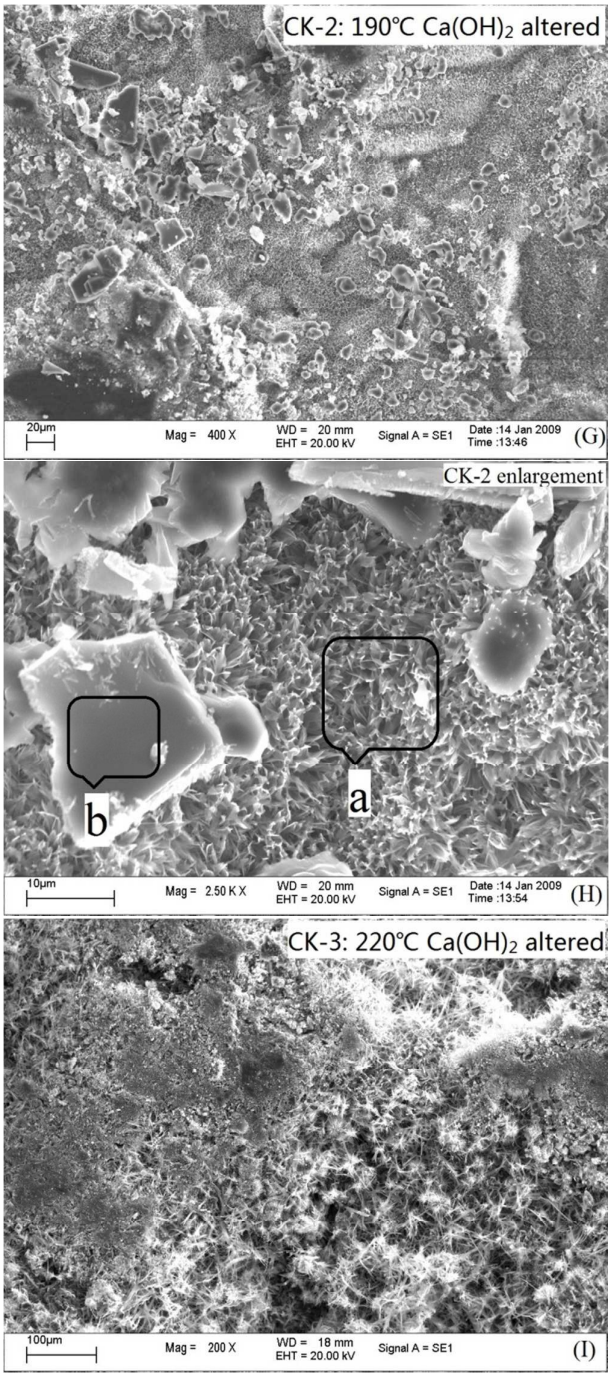

Fig. 1 (G)-(I) SEM of K–feldspar surface: (G) $Ca(OH)_2$-altered K–feldspar at 190 °C (CK–2); (H) Enlargement of CK–2 (CK–2a, fiber; CK–2b, block); (I) $Ca(OH)_2$-altered K–feldspar at 220 °C (CK–3).

process of element dissolution and reprecipitation[17-19, 25-27].

3.2 Decomposition under $Ca(OH)_2$ at different temperatures

When K–feldspar bulk was exposed to $Ca(OH)_2$ solution from 160 °C to 220 °C, the surface of the K–feldspar bulk was greatly changed, and quantities of phases were deposited on the surface. In the filtrate, the amount of Ca was negatively correlated to that of K with increasing temperature (Table 3). When the temperature increased, the decomposition of K–feldspar correspondingly aggravated. As a result, quantities of K^+ were dissolved into the solution, and substantial Ca^{2+} reacted with other ions to form new phases. The amount of Ca^{2+} in the filtrate approached zero when the temperature was increased to 220 °C. Hence, almost all added $Ca(OH)_2$ reacted

with K–feldspar. At 220 °C, some white precipitates (labeled as CK–3P) were found when the solution was filtrated. As temperature increased, the morphology of formed phases appeared diverse (Figs. 1D–N).

K–feldspar bulk was altered by $Ca(OH)_2$ solution at different temperatures. The formed phases were evaluated on the basis of SEM morphology and their chemical compositions measured by EDS. At 160 °C, some fibroid (CK–1a in Table 1S; Fig. 1Ea), spheroidal (CK–1b in Table 1S; Fig. 1Eb), and polyhedral (CK–1c in Table 1S; Fig. 1Fc) phases appeared. The fibroid phase was a transitional compound of $KAlSi_3O_8$ with a few inserted Ca atoms, and the spheroidal phase was hydrogarnet. The polyhedral phase was hypothesized to be calcium silicate hydrate (CSH). However, hydrated calcium silicate form generally appears under hydrothermal condition, and XRPD in Fig. 2 confirmed this conclusion. At 190 °C, a fibroid phase (CK–2a in Table 1S; Fig. 1Ha) and a transitional compound of $KAlSi_3O_8$ with considerable inserted Ca atoms appeared. The fibroid phase appeared similar to some grasses on the lawn. The fibroid phases at 190 °C (CK–2a) and 160 °C (CK–1a) were significantly different, and CK–1a was the same as a honeycomb. The block phase (CK–2b in Table 1S; Fig. 1Hb) was speculated to be CSH, which had a different chemical composition from that of CK–1c. However, hydrogarnet did not appear. The spheroidal phase might be covered by CK–2a and CK–2b when the temperature increased because hydrogarnet was inlayed at the bottom of the honeycomb-like transitional compound of $KAlSi_3O_8$ with a few inserted Ca atoms at 160 °C (CK–1). At 220 °C, a beautiful

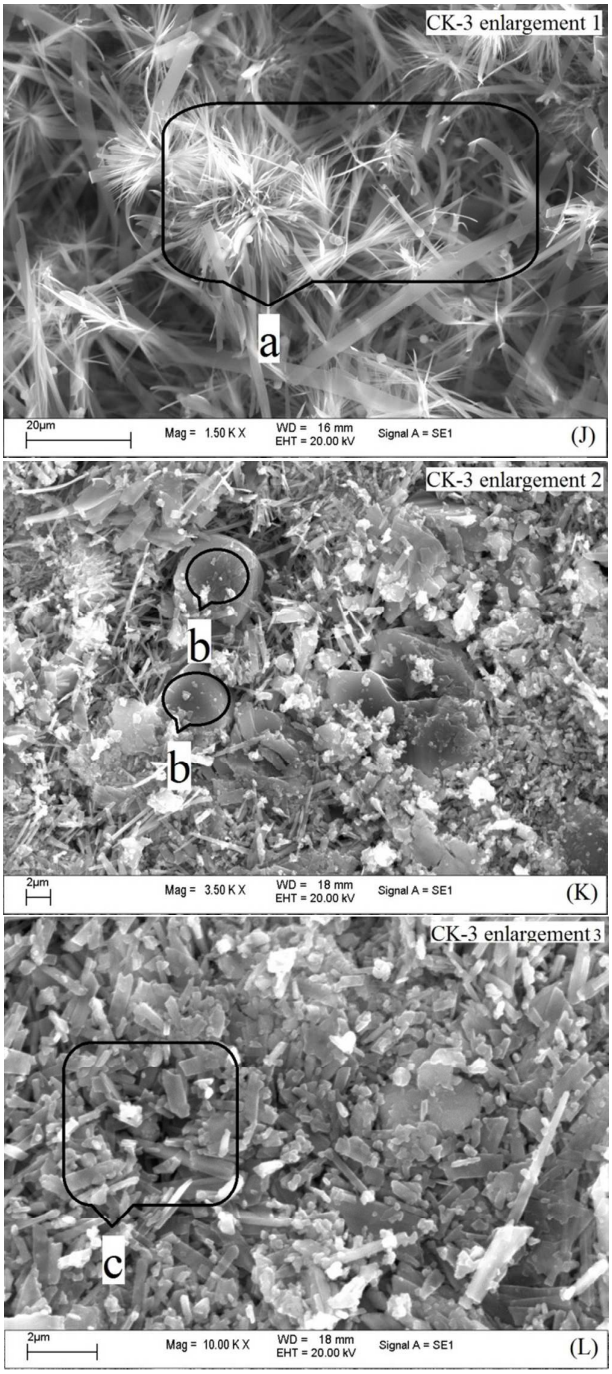

Fig. 1 (J)-(L) SEM of K–feldspar surface: (J) Enlargement part one of CK–3 (CK–3a, fiber); (K) Enlargement part two of CK–3 (CK–1b, octahedron); (L) Enlargement part three of CK–3 (CK–3c, bar).

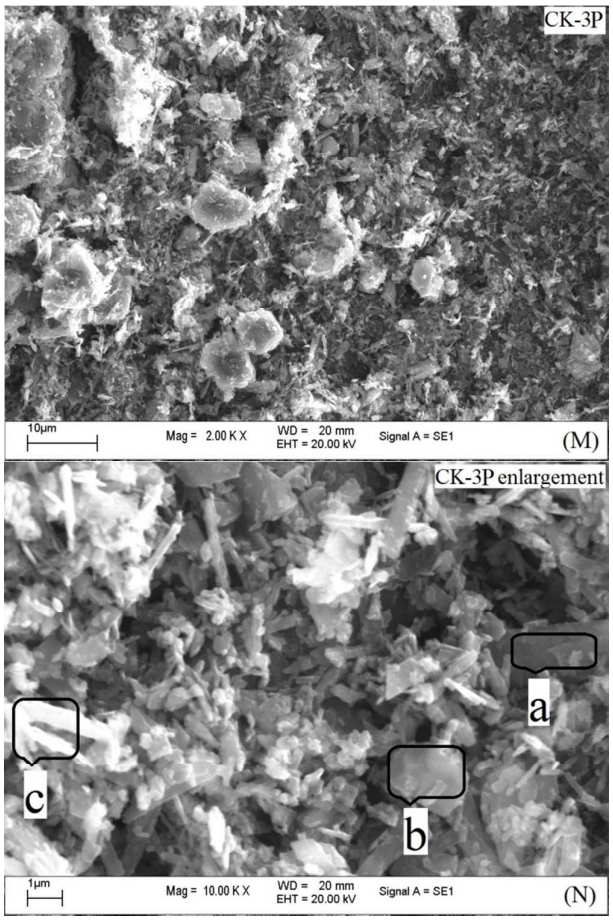

Fig. 1 (M)-(N) SEM of K–feldspar surface: (M) CK–3P (white precipitation in the filtrate of CK–3); (N) Enlargement of CK–3P (CK–3Pa, bar; CK–3Pb, sphere; CK–3Pc, needle).

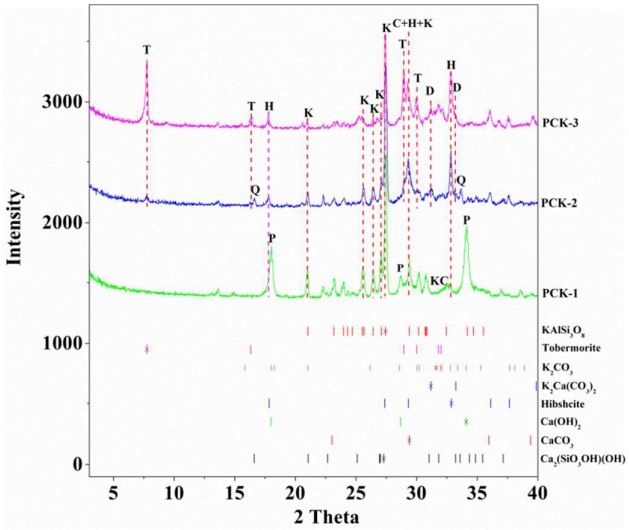

Fig. 2 XRPD pattern of hydrothermal products at different temperatures for PCK–1, PCK–2, and PCK–3. Only the characteristic peaks of each phase were labeled; the vertical bar at the bottom denotes the reference card, and ✳ denotes the strongest peak of the reference card. Abbreviation: K–potassium feldspar ($KAlSi_3O_8$); T–Tobermorite; H–Hibschite; C–Calcite ($CaCO_3$); D–Dipotassium calcium carbonate ($K_2Ca(CO_3)_2$); Q–calcium silicate hydroxide ($Ca_2(SiO_3OH)(OH)$); P–Portlandite ($Ca(OH)_2$).

fibroid phase (CK–3a in Table 1S; Fig. 1Ja) formed, which was tobermorite. The octahedral phase (CK–3b in Table 1S; Fig. 1Kb) was determined to be hydrogarnet. The bar phase (CK–3c in Table 1S; Fig. 1Lc) was concluded to be tobermorite. The bar, spheroidal, and needle phases (CK–3Pa, CK–3Pb, and CK–3Pc in Table 1S, respectively; Figs. 1Na, b, c) of the precipitation in the filtrate were identified to be tobermorite, unconfirmed CSH (UCSH), and tobermorite, respectively. To avoid confusion, the authors defined a few terms for CSH and used the term CSH to specifically imply all CSH phases throughout the remainder of the manuscript. UCSH referred to the phases unconfirmed in this study. When no specific phase was implied, the authors used the term "other CSH (OCSH)."

The morphology of tobermorite changed with different experimental conditions. Bar, needle, and fibroid tobermorites were found in the studies of 5, 11-12, 15, 28-29. Connan *et al.*[30] reported that good crystallinity of tobermorite appeared laminar, whereas poor crystallinity of tobermorite appeared fibroid. Good crystallinity appeared at a higher temperature (CK–3a, CK–3c, and CK–3Pa), which agreed with the conclusion of Connan *et al.*[30]. The fibroid morphology appeared at all three temperatures, and corresponding phases changed from a transitional compound to tobermorite. CK–1c, CK–2b, and CK–3Pb were hypothesized to be UCSHs with different atom ratios, and these phases may be amorphous. Hydrogarnet has been reported to be octahedron[28-29, 31] or spheroidal[5, 11-12, 15, 32].

XRPD results of PCK–1, PCK–2, and PCK–3 showed that the quantity of K–feldspar greatly decreased as temperature increased, and tobermorite and hydrogarnet formed continuously (Fig. 2 and Table 2S). SEM (Fig. 3) showed that

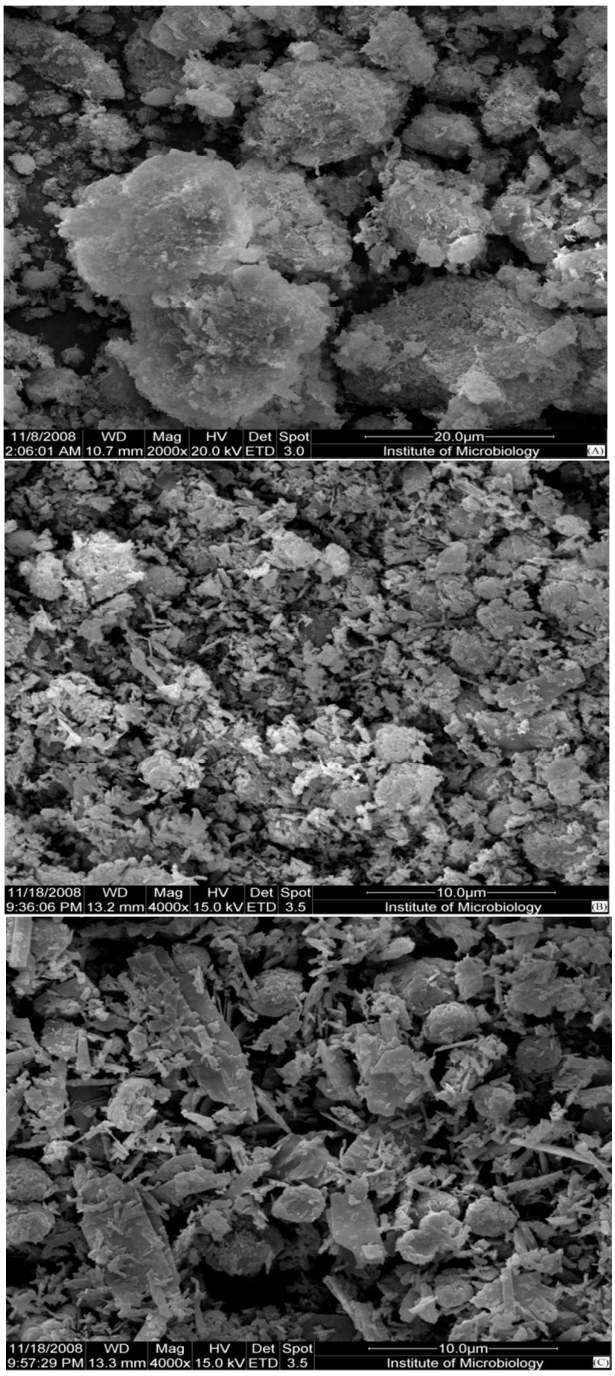

Fig. 3 SEM: (A) PCK–1; (B) PCK–2; (C) PCK–3.

the spheroidal and laminar phases appeared increasingly at higher temperature. EDS measurement proved that the chemical compositions of spheroidal and bar phases approached those of tobermorite and hydrogarnet, respectively. Therefore, tobermorite was laminar, and hydrogarnet was spheroidal for the hydrothermal productions of K–feldspar and CaO powders reaction. Phases containing K element were K_2CO_3 and $K_2Ca(CO_3)_2$, which both formed during water evaporation after the hydrothermal reaction, as validated by XRPD (Fig. 2). KOH formed when K–feldspar

Table 4 Elements measured by ICP–OES and calculated from XRPD

			PCK–1	PCK–2	PCK–3
ICP–OES	Dissolved in deionized water (%)	K_2O	2.20	4.82	4.96
		SiO_2	0.09	0.53	0.53
		Al_2O_3	0.05	0.04	0.03
		CaO	9.00	0.32	0.28
	Dissolved in 0.5 mol/L HCl (%)	K_2O	2.43	5.57	7.28
		SiO_2	10.23	23.01	30.33
		Al_2O_3	2.87	6.47	8.28
		CaO	33.9	34.66	34.45
XRPD		K_2O	3.47	5.00	4.07
		SiO_2	3.07	10.96	27.55
		Al_2O_3	3.41	6.27	7.51
		CaO	30.7	35.35	33.58

reacted with $Ca(OH)_2$, and then KOH reacted with CO_2 to form K_2CO_3 and $K_2Ca(CO_3)_2$. Reardon and Fagan[33] reported $K_2Ca(CO_3)_2$ as a production of $CaCO_3$–KOH system under hydrothermal condition.

For PCK–1, PCK–2, and PCK–3, XRPD showed that all phases, except K–feldspar, can be dissolved in 0.5 mol/l HCl. Thus, K–feldspar was the only residue after the production was dissolved in 0.5 mol/l HCl. The oxide contents calculated from XRPD by the Rietveld method in Table 4 covered all phases, except K–feldspar. The results in Table 4 showed that most of K element was water-soluble, whereas Si and Al were acid-soluble. For K element, the difference between oxides in deionized water and oxides in 0.5 mol/l HCl became significant at higher temperature. The K_2O content calculated from XRPD deviated from the acid-soluble value measured by ICP–OES for PCK–3. In theory, the oxide contents from XRPD should be equal to those dissolved in 0.5 mol/L HCl (%). This deviation may be due to the fact that tobermorite, as a layer silicate, has a high exchangeability and selectivity for cations[34-36]. This characteristic is closely related to the substitute of Al for Si, and some alkali metal ions or alkali earth metal ions, such as Na^+, K^+, and Ca^{2+}, enter into the structure of tobermorite to keep electric neutrality[35, 37-42]. Al-substituted tobermorite possibly formed at 220 °C, and some K ions entered into tobermorite[43]. Therefore, the K_2O content in 0.5 mol/l HCl measured by ICP–OES agreed with the sum that the difference of K element between oxides in 0.5 mol/l HCl and oxides in deionized water was added to the calculated K_2O content from XRPD. The deviation was due to an absence of K element in the chemical formula of tobermorite used to calculate the oxide content by the Rietveld method. The K^+ absorption in tobermorite made part of K slowly release. This feature is important for the utilization of K fertilizer produced from K–feldspar because it will improve the efficiency of K utilization. CaO and Al_2O_3 in 0.5 mol/l HCl measured by ICP–OES were basically in accordance with those calculated from XRPD. Nevertheless, the SiO_2 content calculated from XRPD was obviously less than that measured by ICP–OES for these productions at lower temperature. The underestimation of SiO_2 from XRPD was possibly because some amorphous phases, such as UCSH, were not observed by XRPD. This underestimation was indirectly proven by a closer agreement of SiO_2 content calculated from XRPD and measured by ICP–OES for PCK–3 when substantial crystal phases formed at 220 °C.

3.3 Reaction mechanism

Phases with different morphology on the surface of K–feldspar bulk were evaluated on the basis of their chemical compositions and the morphologies in published papers when K–feldspar bulk reacted with $Ca(OH)_2$ solution at different temperatures. One phase may be covered on another one, which would decrease the accuracy of the chemical composition measured by EDS. For example, hydrogarnet contained some K atoms (Table 1S), which was possibly caused by the low resolution of EDS and/or the deposition of some phases containing K. However, XRPD of powder productions proved that the phases were mainly some CSH phases, including tobermorite and OCSH (crystal or amorphous), hydrogarnet, and KOH when K–feldspar reacted with $Ca(OH)_2$. Analysis of the chemical compositions using SEM and EDS indicated that the identification of these phases from K–feldspar bulk and $Ca(OH)_2$ agreed with the conclusions from the reaction between K–feldspar powder and lime under hydrothermal condition. The phases found in this study also agreed with those reported by Meller *et al.*[44], who presented a detailed study of $CaO–Al_2O_3–SiO_2–H_2O$ system under hydrothermal condition. Therefore, the authors are confident of the efficacy of identifying these phases.

In this study, SEM and the ion amounts measured by ICP–OES showed that reactions significantly differed for K–feldspar attacked by different alkalis, such as NaOH, KOH, and $Ca(OH)_2$. NaOH and KOH hardly decomposed K–feldspar by ion exchange and OH^- alteration under the experimental condition stated in this paper. However, the reaction was accelerated when $Ca(OH)_2$ reacted with K–feldspar to form new phases. This result showed $Ca(OH)_2$ was more active than NaOH and KOH under the stated condition in this paper. The weathering productions of K–feldspar in nature were generally clay minerals, such as kaolinite. The reaction was as follows:

$$4\mathrm{KAlSi_3O_8} + 4H^+ + 2H_2O \xrightarrow[natural\ weathering]{} 4K^+ + Al_4Si_4O_{10}(OH) + 8SiO_2 \quad (1)$$

In this study, the reaction between K–feldspar and $Ca(OH)_2$ from 160 °C to 220 °C can be described using the following expression:

$$2KAlSi_3O_8 + Ca(OH)_2 \xrightarrow[160\sim220\ ℃]{} 2K^+ + [Ca^{2+} \equiv 2AlSi_3O_8^- \equiv xOH^-] \xrightarrow[160\sim220\ ℃]{} hydrogarnet + CSH \quad (2)$$

where CSH denotes the CSH phases, including tobermorite, dicalcium silicate hydrate, and crystal or amorphous OCSH. $[Ca^{2+} \equiv 2AlSi_3O_8^- \equiv xOH^-]$ denotes a transitional compound. Data of EDS showed that the transitional compound had different chemical compositions at different temperatures (Table 1S). An ideal chemical formula, where $[OH^-]$ exists considering that the reaction happened under the hydrothermal condition, was presented to simplify the statement.

As an example, at 220 °C, the equation became

$$2KAlSi_3O_8 + 6.3525Ca(OH)_2 + 0.195H_2O \xrightarrow[220\,℃]{} Ca_3Al_2(SiO_4)_{1.53}(OH)_{5.88} + 1.49Ca_{2.25}(Si_3O_{7.5}(OH)_{1.5}) \cdot H_2O + 2KOH \quad (3)$$

From Eq. (2), the reaction process of K–feldspar and $Ca(OH)_2$ can be described by the following statement: K^+ was dissolved into the solution, and Ca^{2+} reacted with $AlSi_3O_8^-$ and OH^- to form a transitional compound [$Ca^{2+} \equiv 2AlSi_3O_8^- \equiv xOH^-$]; the transitional compound [$Ca^{2+} \equiv 2AlSi_3O_8^- \equiv xOH^-$] further formed hydrogarnet and CSH phases, and CSH phases changed with different temperatures.

Based on XRPD with some published papers, several researchers[5-6, 9-11] proposed that Si-rich/Al-deficient precursor complexes ($SiO_2 \cdot nH_2O$) produced during the reversible exchange of H with Al^{3+} on the surface of K–feldspar under hydrothermal condition, and their proposal was speculated instead of being measured. However, in the current study, a transitional compound [$Ca^{2+} \equiv 2AlSi_3O_8^- \equiv xOH^-$] was observed for the first time.

Hellmann *et al.*[18] used high-resolution transmission electron microscopy (TEM) and energy-filtered TEM (EFTEM) to study mineral-fluid interfaces using TEM foils cut directly across the reaction boundaries and in the cross section at nanometer to sub-nanometer resolutions. They directly measured the surface chemistry and structure of a large suite of laboratory-altered and field-weathered silicate minerals. Their results indicated a general presence of surface layers composed of amorphous and hydrated silica. It is difficult for powder reaction using the measurement made by Hellmann *et al.*[18] through TEM and EFTEM to check the surface of the solid phase because of the deposition of newly formed phases[5-6, 9-11]. Furthermore, it is not the key point to discuss the weathering mechanism of feldspar in this paper. However, the authors agreed with the conclusion of Hellmann *et al.*[18] that dissolution-reprecipitation is a universal mechanism that controls fluid-mineral interactions, and a chemical weathering continuum exists on the fluid-mineral interface (please refer to Fig. 4 in Hellmann et al.'s paper). The chemical weathering continuum was based on interfacial dissolution-reprecipitation as the principal mechanism of chemical weathering. The mineral-mineral replacement reaction for a natural mineral-fluid system is common by a dissolution-reprecipitation mechanism, and it has been advocated by some authors (please refer to reviews in 25-27, for more details). The generation of porosity during replacement processes, as a common phenomenon, has been reported in many systems, both in experiments and in nature (e.g., see 25-26, 45-47), including feldspars[48-51]. SEM (Fig. 1) showed that the formation of porosity accompanied the generation of new phases when K–feldspar bulk reacted with $Ca(OH)_2$ at different temperatures. However, the porosity was absent for NK and KK because no new phase appeared. Porosity is important for the application of K–feldspar as a fertilizer, which will be beneficial to preserve water and nutrients in soil and to improve the physical and chemical characteristics of soil. The decomposition of K–feldspar bulk or powder with lime is also a "pressure-tight interfacial mineral-fluid" reaction. Lime first reacts with water to form $Ca(OH)_2$, and K–feldspar then reacts with $Ca(OH)_2$ to generate new phases. Hence, the interface-coupled dissolution-precipitation mechanism occurs between K–feldspar solid and $Ca(OH)_2$ aqueous solution. $Ca(OH)_2$ aqueous solution will induce some composition dissolution in K–feldspar solid (Table 1S), thereby producing an interfacial boundary layer of fluid that may be supersaturated with respect to one or more stable phases. One of these phases may then nucleate at the surface of the parent phase to initiate an autocatalytic reaction that couples the dissolution and precipitation rates. If an epitaxial crystallographic matching exists between the parent substrate and the product, the nucleation of the new phase transfers crystallographic information from parent to product. Mass transfer pathways must be maintained between the fluid reservoir and the reaction interface to propagate a mineral-mineral replacement reaction. Consequently, the replacement process is a volume deficit reaction, and the resulting product is porous (Fig. 1), thus allowing continued infiltration of the fluid phase to the interface with the parent phase. At 220 °C, some white precipitations were found at the filtrate of CK–3, but white precipitations did not appear at 160 and 190 °C. This phenomenon was in accordance with the ongoing proceeding of the mineral-mineral replacement reaction. A similar experiment was performed by Dunkel and Putnis[45]. They used single crystals of scolecite ($CaAl_2Si_3O_{10} \bullet 3H_2O$) to interact with NaCl and NaOH solutions of different concentrations and pH values in autoclaves at temperatures up to 200 °C. Only the experiments with 1 or 2 M NaOH at 200 °C led to significant reactions, namely, one or two reaction rims, depending on the reaction time. At all reaction times, however, a reaction rim consisting of Na and Al-substituted tobermorite (11 Å) ($Ca_{4.5}Na_{1.3}Si_{5.2}Al_{1.0}O_{16}(OH)_2$) formed. The reaction interfaces were sharp, and the product phases formed porous pseudomorphs of the original scolecite. Their results indicated that replacement of scolecite occurred by coupled dissolution-precipitation. In this study, a direct observation of the sharp reaction interface was absent, however, based on the great similarity between Dunkel and Putnis's experiment[45] and the experiment in the current study and the above statement, the authors concluded that the K–feldspar decomposition was also a mineral-mineral replacement reaction by the dissolution-precipitation mechanism.

A K–feldspar decomposition model is presented in this paper, and a comparison of the presented model in this study and the chemical weathering continuum model in the report of Hellmann *et al.*[18] is shown in Fig. 4. To some extent, the decomposition process of K–feldspar and lime under hydrothermal condition was similar to the chemical weathering process implied by the chemical weathering continuum model of Hellmann *et al.*[18]. When the hydrothermal reaction of K–feldspar and lime occurred, the surface of K–feldspar under hydrothermal condition possibly had a similar structure to that of chemical weathering K–feldspar. Although the chemical weathering of feldspar spread in a long period and the hydrothermal decomposition of K–feldspar only needed a few to tens of hours, the nature of K–feldspar decomposition under both conditions was a mineral-mineral

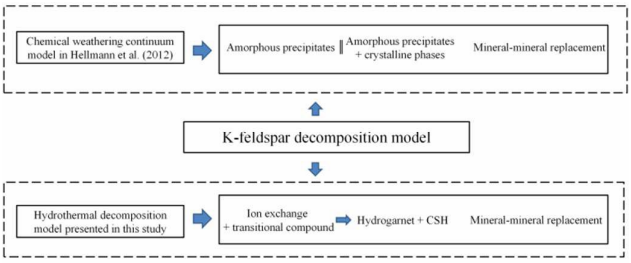

Fig. 4 Comparison of the chemical weathering continuum model in Hellmann *et al.*[18] and the hydrothermal decomposition model presented in this study.

replacement reaction.

4. Conclusions

In this study, the reactions between K–feldspar and alkalis were systematically investigated using K–feldspar bulk and powder under hydrothermal condition. Various techniques, such as SEM, EDS, ICP–OES, XRPD, and the Rietveld method, were used. The deposition of secondary phases on the surface of K–feldspar bulk was observed by SEM. $Ca(OH)_2$ was more active than NaOH and KOH under the stated conditions because $Ca(OH)_2$ can react with K–feldspar to form new phases. The morphologies of newly formed phases were diverse when K–feldspar reacted with $Ca(OH)_2$ at different temperatures. A transitional compound [$Ca^{2+}{\equiv}2AlSi_3O_8^-{\equiv}xOH^-$] was observed for the first time. Hydrogarnet appeared from 160 °C to 220 °C, and tobermorite began to form at 190 °C. Some K and Al atoms may enter into the structure of tobermorite at a higher temperature.

A model of K–feldspar decomposition under hydrothermal condition was presented, which had a similar process to the chemical weathering of K–feldspar, both being a mineral-mineral replacement reaction by the dissolution-precipitation mechanism.

Studies of K–feldspar hydrothermal reaction provided important and meaningful hints on the utilization of K–feldspar as a fertilizer, e.g., tobermorite, as a layer silicate, has high exchangeability and selectivity for cations, which can alleviate the damage of heavy metals, such as Cd, Pb, and Cr, on soil[52-53], and it is also a slow-release reservoir for some nutrients, such as K^+. The porosity of newly formed phases will also improve the physical and chemical characteristics of soil because of its permeability and potential capability of preserving moisture and fertility. Further, tobermorite, as a primary production of K–feldspar and lime hydrothermal reaction, has a similar structure to that of the 2:1 clay minerals, which plays a key role in soil K cycle[54], and is also very helpful in keeping an ecological balance when the production obtained from K–feldspar and lime hydrothermal reaction as an alternative to K salts is fertilized into the soil. Thus, the potential application of activated K–feldspar as a fertilizer in agriculture, such as zeolite with similar characteristics, will be gradually realized in future. Understanding the role of K–feldspar in keeping the ecological balance of the Earth during weathering is helpful given its large amount.

Acknowledgements

This research project was supported by Projects in the National Science & Technology Pillar Program during the Eleventh Five-Year Plan Period **(**China, No. 2006BAD10B04) and the Knowledge Innovation Project of Chinese Academy of Sciences and Spark Program of China (No. 2007EA173003). Two anonymous reviewers are thanked for their constructive critical suggestions aimed to improve the quality of the manuscript.

Notes and references

‡Tables 1S and 2S were deposited as supplementary files.

1 J.M. Liu, S. K. Liu, C. Han, X. B. Sheng, X. Qi and Z. L. Zhang, *Bulletin of Mineralogy Petrology and Geochemistry*. 2014, **33(5)**, 556–560.
2 D. A. C. Manning, *Agron. Sustain. Dev.* 2010, **30**, 281–294.
3 C. Han, *patent*. 2007, CN200710098753.0, China (Chinese).
4 C. Han and J. M. Liu, *patent*. 2007, CN200710178794.0, China (Chinese).
5 H. Liu, Synthesis of tobermorite powder from potassium feldspar: Reactive mechanism research, *Dissertation, China University of Geosciences*. 2006, Beijing, China (Chinese).
6 H. Liu, H. W. Ma, Y. M. Nie and L. Wang, *Geoscience.* 2006, **20(2)**, 347–353 (Chinese).
7 Y. Q. Liu, H. T. Xia and H. W. Ma, *Advanced Materials Research.* 2012, **549**, 65–69.
8 H. W. Ma, J. Yang, Y. B. Wang, G. Wang, S. D. Miao, W. W. Feng, Q. X. Ding, *Earth Science —Journal of China University of Geosciences.* 2007, **32(01)**, 111–118 (Chinese).
9 Y. M. Nie, Mineral Polymer in the System of SiO_2–Al_2O_3–$Na_2O(K_2O)$–H_2O: Preparation and Reaction Mechanism, *Dissertation, China University of Geosciences*. 2006, Beijing, China (Chinese).
10 Y. M. Nie, H.W. Ma, H. Liu, P. Zhang, M. Y. Qiu and L. Wang, *Journal of the Chinese Ceramic society.* 2006, **34(7)**, 846–850, 867 (Chinese).
11 M. Y. Qiu, Synthesis of tobermorite by dynamical decomposing potassium feldspar: an experimental study, *Dissertation, China University of Geosciences*. 2005, Beijing, China (Chinese).
12 M. Y. Qiu, H. W. Ma, Y. M. Nie, P. Zhang and H. Liu, *Geoscience.* 2005, **19(03)**, 348–354 (Chinese).
13 T. Skorina and A. Allanore, *International publication number*. 2014, WO2014182693 A1, US.
14 Y. J. Yan and J. X. Lan, *High Technology Letters.* 1994, **8**, 26–28 (Chinese).
15 P. Zhang and H. W. Ma, *Acta Petrologica Et Mineralogica.* 2005, **24(4)**, 333–338 (Chinese).
16 H. Q. Zhao, C. J. Hu, H. L. Ma, L. Z. Wang, J. Li and Y. X. Liu, *China's Manganese Industry.* 2002, **20(01)**, 27–29, 43 (Chinese).
17 E. S. Chardon, F. R. Livens, and D. J. Vaughan, *Earth-Sci. Rev.* 2006, **78(1–2)**, 1–26.
18 R. Hellmann, R. Wirth, D. Daval, J. P. Barnes, J. M. Penisson, D. Tisserand, T. Epicier, B. Florin and R. L. Hervig, *Chem. Geol.* 2012, **294–295**, 203–216.
19 T. Skorina and A. Allanore, *Green Chem.* 2015, **17**, 2123–2136.
20 A. C. Lasaga, *J. Geophys. Res.* 1984, **89**, 4009–4025.
21 A. C. Larson and R. B. Von Dreele, General Structure Analysis System (GSAS), *Los Alamos National Laboratory Report.* LAUR, 2004, 86–748.
22 B. H. Toby, *J. Appl. Crystallogr.* 2001, **34**, 210–213.
23 H. M. Rietveld, *J. Appl. Crystallogr.* 1969, **2**, 65–71.

24 S. Q. Su, H. W. Ma, J. Yang, H. Liu and G. Li, *Journal of the Chinese Ceramic society.* 2012, **40(1)**, 145–148.
25 A. Putnis, *Mineral. Mag.* 2002, **66**, 689–708.
26 A. Putnis, Mineral replacement reactions. In: Oelkers, E.H., Schott, J. (Eds.), *Thermodynamics and Kinetics of Water – Rock Interaction.* Mineralogical Society America, Washington, D.C., 2009, pp. 87–124.
27 E. Ruiz–Agudo, C. V. Putnis and A. Putnis, *Chem. Geol.* 2014, **383**, 132–146.
28 D. S. Klimesch and A. Ray, *Cem. Concr. Res.* 1998, **28(8)**, 1109–1117.
29 D. S. Klimesch and A. Ray, *Cem. Concr. Res.* 1998, **28(9)**, 1317–1323.
30 H. Connan, D. Klimesch, A. Ray and P. Thomas, *J. Therm. Anal. Calorim.* 2006, **84(2)**, 521–525.
31 S. Fujita, K. Suzuki and Y. Shibasaki, *J. Mater. Cycles Waste Manag.* 2002, **4**, 41–45.
32 D. S. Klimesch and A. Ray, *Advanced Cement Based Materials*. 1998, **7(3–4)**, 109–118.
33 E. J. Reardon and R. Fagan, *Appl. Geochem.* 2000, **15**, 327–335.
34 S. V. Churakov, *Eur. J. Mineral.* 2009, **21(1)**, 261–271.
35 S. Komarneni and D. M. Roy, *Science.* 1983, **221(4611)**, 647–648.
36 S. Merlino, E. Bonaccorsi, M. Merlini, F. Marchetti and W. Garra, *Minerals as Advanced Materials*. 2008, **I**. 37–44.
37 S. Komarneni, E. Breval, M. Miyake and R. Roy, *Clay Clay Min.* 1987, **35(5)**, 385–390.
38 S. Komarneni and D. M. Roy, *J. Mater. Sci.* 1985, **20(8)**, 2930–2936.
39 S. Komarneri, D. M. Roy and R. Roy, *Cem. Concr. Res.* 1982, **12(6)**, 773–780.
40 S. Komarneni and M. Tsuji, *J. Am. Ceram. Soc.* 1989, **72(9)**, 1668–1674.
41 M. Tsuji and S. Komarneni, *J. Mater. Res.* 1989, **4**, 698–703.
42 M. Tsuji, S. Komarneni and P. Malla, *J. Am. Ceram. Soc.* 1991, **74(2)**, 274–279.
43 N. Organova, E. V. Koporulina, A. G. Ivanova, N. V. Trubkin, A. E. Zadov, A. P. Khomyakov, I. M. Marcille, N. V. Chukanov and A. N. Shmakov, *Crystallogr. Rep.* 2002, **47(6)**, 1020–1026.
44 N. Meller, K. Kyritsis and C. Hall, *Cem. Concr. Res.* 2009, **39(1)**, 45–53.
45 K. G. Dunkel and A. Putnis, *Eur. J. Mineral.* 2014, **26**, 61–69.
46 R. Lafay, G. Montes-Hernandez, E.Janots, R. Chiriac, N. Findling and F. Toche, *J. Cryst. Growth.* 2012, **347**, 62–72.
47 A. Putnis and C. V. Putnis, *J. Solid State Chem.* 2007, **180**, 1783–1786.
48 F. David, F. D. L. Walker, M. R. Lee and I. Parsons, *Mineral. Mag.* 1995, **59**, 505–534.
49 A. Putnis, R. Hinrichs, C. V. Putnis, U. Golla–Schindler and L. Collins, *Lithos*. 2007, **95**, 10–18.
50 C. V. Putnis, T. Geisler, P. Schmid-Beurmann, T. Stephan and C. Giampaolo, *Am. Miner.* 2007, **92**, 19–26.
51 R. H. Worden, F. D. L. Walker, I. Parsons, W. L. Brown, *Contrib. Mineral. Petrol.* 1990, **104**, 507–515.
52 N. J. Coleman, *Sep. Purif. Technol.* 2006, **48(1)**, 62–70.
53 R. Pena, A. Guerrero and S. Goni, *J. Hazard. Mater.* 2006, **129(1–3)**, 151–157.
54 P. Hinsinger. Potassium, R. Lal (Ed.), *Encyclopedia of Soil Science*, Marcel Dekker, Inc., 2002, New-York, USA.